Synthesis, characterization and antimicrobial activity of bis(phthalazine-1-hydrazone)-2,6-diacetylpyridine and its complexes with Co^{III}, Ni^{II}, Cu^{II} and Zn^{II}

Berta Holló[a], József Magyari[a], Vukadin M. Leovac[a], Vukosava Živković-Radovanović[b], Gordana Vučković✝[b], Zoran D. Tomić[c], Imre Miklós Szilágyi[d], György Pokol[d], Katalin Mészáros Szécsényi[a*]

[a]Faculty of Sciences, University of Novi Sad, Trg Dositeja Obradovića 3, 21000 Novi Sad, Serbia
[b]Faculty of Chemistry, University of Belgrade, P.O. Box 51, 11158 Belgrade, Serbia
[c]Vinča Institute of Nuclear Sciences, University of Belgrade, P.O.Box 522, 11001 Belgrade, Serbia
[d]Department of Inorganic and Analytical Chemistry, Budapest University of Technology and Economics

Abstract

Four new complex compounds of bis(phthalazine-1-hydrazone)-2,6-diacetylpyridine (Hz_2DAP) ligand with Ni^{II}, Co^{III}, Cu^{II} and Zn^{II} metal centres with potential biological activity, were synthesized and characterized by single-crystal X-ray diffraction and IR spectral data. The structure of the Zn^{II} complex is determined on the basis of the IR spectral and thermal data. The antimicrobial activity of Hz_2DAP and its complexes [Co(Hz_2DAP-H)Cl$_2$]·MeOH, [Ni(Hz_2DAP-H)]Cl·MeOH, [Cu(Hz_2DAP-H)Cl] and [Zn(Hz_2DAP-2H)]·H$_2$O were tested in vitro against selected gram($-$) and gram(+) bacterial strains and fungi. The antimicrobial activity of the ligand is negligible, while its complexes with Ni^{II}, Co^{III} and Cu^{II} show considerable activity against *Escherichia coli*, *Staphylococcus aureus* and *Micrococcus lysodeikticus*. On the contrary, [Zn(Hz_2DAP-2H)]·H$_2$O promotes the growth of *Candida albicans*, while its antibacterial activity is negligible. On the basis of thermal data and those from coupled TG/MS measurements the decomposition mechanism were determined and evaluated. The thermal data were used also to support the proposed structure of [Zn(Hz_2DAP-2H)]·H$_2$O.

Keywords: bis(phthalazine-1-hydrazone)-2,6-diacetylpyridine, Ni^{II}, Co^{III}, Cu^{II} and Zn^{II} complexes, antimicrobial activity, TG/MS

---

[*]Corresponding author: K. Mészáros Szécsényi, Phone: +381/21-485-2740, e-mail: mszk@uns.ac.rs

Introduction

Hypotensive 1-hydrazinophthalazine known as Hydralazine® (Hz) was used in therapy of hypertension from 50's of the last century. It is also an excellent ligand and forms chelates with transition metals including Fe^{II} and Co^{II}. However, it was not proved yet that the complex formation capability is connected to its hypotensive activity [1]. By condensation with Schiff bases hydralazine readily gives hydrazones with also good coordination ability. The complex formation of Cu^{II} with polyfunctional binucleating pyridyl phthalazine and phthalazine-hydrazone was extensively studied by L. K. Thomson *et. al.* for more than 20 years, mostly because of their interesting magnetic properties [2,3]. The number of papers referring to phthalazine-hydrazone complexes decreased in 90's but from the beginning of the 21th century, mostly due to their significant biological activity, research activities dealing with this type of complexes is increasing [4–9]. V.A. Kogan *et. al.* in a review paper discuss the relationship between the structure and biological activity of phthalazine hydrazones and their complexes [10].

The ligand, bis(phthalazine-1-hydrazone)-2,6-diacetylpyridine (Hz_2DAP), a derivative of 1-hydrazinophthalazine and its complexes with Ni^{II}, Cu^{II} and Zn^{II} were characterized [11] with the aim to explore the possible coordination modes of the ligand. In the present publication the synthesis, structure and microbial activity of the ligand and its new complexes with Ni^{II}, Co^{III}, Cu^{II} and Zn^{II} are described and discussed, focusing on the structure – activity relationships. As the thermal behaviour of potential drug components is of practical importance [12–16], the thermal decomposition of the compounds is studied in detail.

Experimental

Synthesis of the ligand: 1-Hydrazinophtalazine (5 mmol, 1.00 g) was dissolved in the mixture of 30 cm^3 methanol and 5 cm^3 distilled water with mild heating. To this solution 2,6-diacetylpyridine (2.5 mmol, 0.41 g) dissolved in 10 cm^3 methanol was added. The reaction mixture was refluxed for 30 minutes. After cooling the amorphous orange precipitate is filtered off, washed with methanol and air dried. Yield: 90 %.

Synthesis of the complexes: Solution of $M(CH_3COO)_2 \cdot xH_2O$ (0.2 mmol, M = Co, Ni, Cu and Zn) in 10 cm^3 methanol was added to warm suspension of $Hz_2DAP \cdot 2HCl$ (0.2 mmol) in 15 cm^3 methanol. The reaction mixture was heated until boiling and left at room temperature for ~30 h. The crystalline precipitate (dark brown for Co, Ni and Cu, red-orange for Zn) was filtered off, washed with methanol and dried on air.

Complex $[Zn(Hz_2DAP\text{-}2H)] \cdot H_2O$ was also synthesized by the following procedure: $ZnCl_2$ (0.2 mmol, 0.027 g) dissolved in 10 cm^3 methanol was added to the warm suspension of $Hz_2DAP \cdot 2HCl$ (0.2 mmol, 0.104 g) in 15 cm^3 methanol. The mixture is left to cool to room temperature and 3 cm^3 $NH_{3(aq)}$ was added. Short afterthe formation of amorphous orange precipitate is observed. Next day it was filtered off, washed with methanol and air dried.

Experimental data

$Hz_2DAP \cdot 2HCl$: Yield: 90 %, $M_r = 520.42$

$[Co(Hz_2DAP\text{-}H)Cl_2] \cdot MeOH$ (**1**): Yield: 53 %; $M_r = 608.38$ $gmol^{-1}$; $\lambda_M(DMF) = 5.3$ Scm^2mol^{-1}, IR (cm^{-1}): 1596, 1541, 1504, 1487, 1419, 1390, 1334, 1280, 1249, 1222, 1184, 1154, 1098, 1069, 1033, 694.

$[Ni(Hz_2DAP\text{-}H)]Cl \cdot MeOH$ (**2**): Yield: 48 %; $M_r = 572.68$ $gmol^{-1}$; $\lambda_M(DMF) = 95.0$ Scm^2mol^{-1}, IR (cm^{-1}): 1587, 1548, 1518, 1463, 1404, 1371, 1325, 1274, 1251, 1218, 1180, 1149, 1120, 1071, 1021, 765.

$[Cu(Hz_2DAP\text{-}H)Cl]$ (**3**): Yield: 51 %; $M_r = 545.49$ $gmol^{-1}$; $\lambda_M(DMF) = 14.0$ Scm^2mol^{-1}, IR (cm^{-1}): 1589, 1547, 1514, 1467, 1411, 1378, 1325, 1275, 1240, 1186, 1150, 1093, 1051, 963, 803, 752.

$[Zn(Hz_2DAP\text{-}2H)] \cdot H_2O$ (**4**): Yield: 66 %; $M_r = 528.89$ $gmol^{-1}$; $\lambda_M(DMF) = 7.6$ Scm^2mol^{-1}, IR (cm^{-1}): 1586, 1541, 1489, 1410, 1377, 1321, 1290, 1247, 1138, 1087, 1046, 1017.

Simultaneous TG/DSC measurements were carried out using TA Instruments Q600 SDT thermal analyzer. Sample mass: ~3 mg. Heating rate: 20 ^{o}C min^{-1}. Carrier gases: air, nitrogen. Gas flow rate: 100 cm^3min^{-1}. Sample holder/reference: alumina crucible/empty alumina crucible.

For collecting TG/DTA-MS data TA Instruments SDT 2960 DTA/TGA was used online coupled with Balzers Instruments ThermoStar GSD 300T quadrupole mass spectrometer also at 10 ^{o}C min^{-1} heating rate in N_2 atmosphere at gas flow rate of 130 cm^3min^{-1}. Selected ions between $m/z = 1$–130 were monitored through 64 channels in Multiple Ion Detection Mode (MID) with a measuring time of 0.5 s per channel.

The ligand and the compounds for antimicrobial *in-vitro* activity were tested against the Gram(–) bacterium *Escherichia coli* ATCC 25922 and for Gram(+)bacteria *Staphylococcus aureus* ATCC 25923, *Bacillus subtilis* ATCC 6633, *Bacillus cereus* ATCC 14579 and fungi *Micrococcus lysodeikticus* ATCC 4698; yeast *Candida albicans* ATCC 24433 and mould *Aspergillus niger* ATCC 12066. For tests the method of diffusion in agar was applied [17–18]. The bacteria were cultivated on LAB 8 nutrient agar and fungi on LAB 37 malt extract agar. Equimolar stock solutions ($1.0 \cdot 10^{-3}$ molL^{-1}) of all complexes and the ligand in DMSO were tested for the above listed microorganisms. Blanc tests were performed with pure DMSO (solvent) and the corresponding metal chlorides of the same $1.0 \cdot 10^{-3}$ molL^{-1} concentration in DMSO. After incubation time the diameters of the obtained zones (bactericidal, bacteriostatic, fungistatic) were measured. As no microbial activity was found for the ligand, in further experiments the equimolar stock solutions of the complexes were diluted ten times with deionized water. For the minimum inhibitory concentrations (MIC) determination in the cases were high activity was found, the solutions of concentration $1.0 \cdot 10^{-4}$ mol L^{-1} in DMSO:H$_2$O = 1:9 were additionally diluted with water.

Crystallography

Single-crystal X-ray diffraction data for compounds **1,2** and **3** were collected on an Oxford Diffraction Gemini S four-circle diffractometer equipped with a Sapphire CCD detector, using graphite-monochromated MoKα radiation (λ=0.71073Å) at room temperature. The data reduction was done using the Oxford Diffraction program CRYSALISPRO [19]. Empirical absorption correction using spherical harmonics implemented in the SCALE3 ABSPACK [**Hiba! A könyvjelző nem létezik.**] scaling algorithm were applied. The structures for compounds **1–3** were solved by direct methods using the SIR92 [20] program as implemented in WinGX [21] program system. Structural refinements were done by full-matrix least-squares method based on F^{2}using SHELXL-97 [22]. The hydrogen atoms were placed in the idealized positions and refined using a riding model. At this point, examination of the refined structures indicates presence of voids containing unresolved electron density peaks in the crystal structures of **1** and **2**. Both crystals for the X-ray analysis were grown from methanol, whose presence in the crystal structure was proved also by coupled thermogravimetric/mass spectrometric analysis. However attempts to model the disordered solvent were not successful since this region appears to be only partially occupied and the solvent molecule significantly disordered. The SQUEEZE function of PLATON [23] was used to eliminate the contribution of the solvent molecules and the solvent-free model was used in the final refinement. Geometrical calculations were carried out using the programs PARST [24] and PLATON [**Hiba! A könyvjelző nem létezik.**]. For the structure drawings the programs CAMERON [25] and ORTEP [26] were employed. Crystallographic data for compounds **1**, **2** and **3** have been deposited with the Cambridge Crystallographic Data Centre as CCDC 955435, CCDC 952294 and CCDC 952347, respectively. The data can be obtained free of charge at www.ccdc.cam.ac.uk/conts/retrieving.html.

Crystal data: **1** – C$_{25}$H$_{20}$Cl$_2$CoN$_9$, M = 576.33, orthorhombic, *Pna2$_1$*, a = 20.4039(15) Å, b = 8.6459(5) Å, c = 15.0613(13) Å, V = 2657.0(3) Å^3, Z = 4, 5524 unique reflections were used in calculations. wR = 0.1090 and R = 0.0523 ($I > 2\sigma(I)$).

2 – C$_{25}$H$_{20}$ClNiN$_9$, M = 540.64, monoclinic, *P2$_1$/c*, a = 11.236(5) Å, b = 11.387(5) Å, c = 21.227(5) Å, β = 100.420(5)^o, V = 2671.1(18) Å^3, Z = 4, 5312 unique reflections were used in calculations. wR = 0.1209 and R = 0.0432 ($I > 2\sigma(I)$).

**3** – C$_{25}$H$_{20}$ClCuN$_9$, M = 545.50, monoclinic, *P2$_1$/n*, a = 10.7284(6) Å, b = 16.5948(7) Å, c = 14.2276(8) Å, β = 108.010(6)^o, V = 2408.9(2) Å^3, Z = 4, 4782 unique reflections were used in calculations. wR = 0.1645 and R = 0.0483 ($I > 2\sigma(I)$).

Results and discussion

The ligand (Scheme 1) contains 7 nitrogens as potential donor atoms. However, because of steric effects, with the first row transition metals actually it is a tetradentate ligand. In addition, two NH-groups are also proton donors. As the ligand crystallizes with two HCl molecules, it means that two nitrogen atoms are additionally protonated. Therefore, the complex formation could be promoted by bases. Indeed, using acetate salts of Cu^{II}, Co^{II} and Ni^{II} the corresponding metals complexes with a single deprotonated ligand are formed and precipitated as small, crystalline solids and the molecular structure of the compounds was determined. As the stability of Co^{III} complexes is usually higher, during complex formation the oxidation of Co^{II} to Co^{III} takes places.

With zinc(II) acetate the quality of the crystals were too poor for the structure determination. In order to slow the crystallization rate, for the synthesis instead of zinc acetate, to the cold, clear mixture of zinc chloride and Hz$_2$DAP

solutions ammonia was added, hoping that ammonia would promote the deprotonation of the ligand, while the zinc ammine complex formation slow the precipitation rate allowing thus formation of larger crystals. Unfortunately, the obtained crystals were not suitable for the structure determination, which according to the IR-spectrum of the compound, is identical with that obtained using zinc acetate as staring salt. However, the yield and the purity of the complex are higher if synthesized using ammonia.
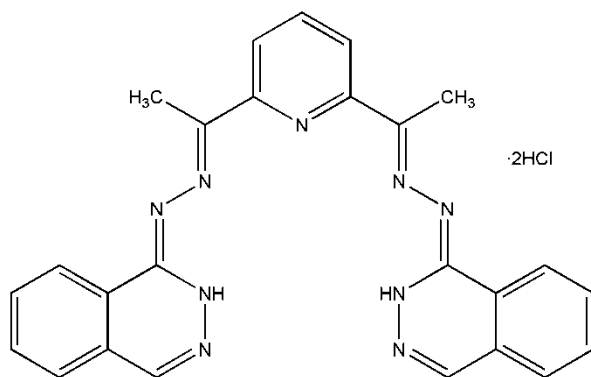
Scheme 1 Bis(phthalazine-1-hydrazone)-2,6-diacetylpyridine (Hz$_2$DAP) ligand

Crystal and molecular structure of 1–3

In all three complexes Hz$_2$DAP is coordinated in the same manner. The mono-deprotonated ligand coordinates through the pyridine nitrogen (N5), two hydrazonic nitrogen (N6, N4) and nitrogen from the deprotonated phthalazine moiety (N8). The molecular diagram and atom numbering scheme of **1–3** are presented in Fig 1. Methyl and methylene hydrogens are excluded for clarity, while hydrogen bond is depicted as dotted line (Fig 1). Four coordinated N atoms are in essentially planar arrangement in all three complexes. Metal atom deviates from the plane consisting of the four coordinated N atoms by 0.0180(7), 0.0671(4) and 0.2095(5) Å in **1**, **2** and **3**, respectively. While the coordination behaviour of the Hz$_2$DAP is determined primarily by its stereochemical properties and degree of protonation, the completion of the coordination sphere depends on the bonding properties of the metal. So it is not unusual that the coordination sphere of the metals in **1**, **2** and **3** is different in spite of the same synthetic procedure and same degree of protonation of the ligand. In **1**, octahedral coordination of Co^{III} is completed by terminal chloride ions in axial positions. The Co–Cl distances are 2.234(1) and 2.264(2)Å. In **2**, Ni^{II} is coordinated in a square-planar fashion by the four N-donors of the Hz$_2$DAP. Distance between the nickel and the closest chlorine is 3.080(2) Å which is above the maximum reported value of 2.841 Å [27] for the Ni-Cl bond, according to data stored in CSD [28]. In **3**, Cu^{II} adopts square-pyramidal geometry, with four N donors of Hz$_2$DAP in equatorial plane and Cl in apical position. The non-coordinated phthalazine moiety is positioned so that the torsion angle N4–N3–C1–C2 is 171.8(4), –170.4(3) and –172.1(3)° in **1**, **2** and **3**, respectively, which is associated with formation of the N–H...Cl hydrogen bond (Fig 1). Regarding the coordination behaviour of Hz$_2$DAP it is interesting to note that the same pattern of M–N bond lengths is observed in all three complexes with M–N4 being the longest and M–N8 the second longest bond (Table 1). Also, the angle formed by these two bonds show the largest deviation from the ideal value. Regarding the difference between the M–N bond lengths (Table 1) it is significant to note that the shortest bond with the metal center is that formed with pyridine nitrogen (N5) which belongs to the condensed aromatic and chelate ring system, while the longest M–N bond is formed with N4 that participates in one chelate ring only. Selected bond distances and angles are given in Table 1. In all three **1–3** complexes the same bond pattern in the Hz$_2$DAP is preserved, with double bonds located at N1–C8, N3–C1, N4–C9, C10–N5, N6–C15 and N9–C23 (Fig 1). This bond pattern resembles the one found in the crystal structure of a

binuclear Ni complex with the same ligand [**Hiba! A könyvjelző nem létezik.**] with one significant distinction. In **1–3** there is a localized C10–N5 double bond in the pyridine ring [range from 1.319(5) to 1.328(4)Å], while in the binuclear Ni complex equivalent values are 1.36(1)–1.37(1) Å, indicating the absence of double bond localization and are in accordance with viewing the whole pyridine ring as a delocalized system. This difference in the bond pattern is related to the different bond lengths between the Ni and pyridine N atom. In **1–3**, the metal–N(pyridine) bond range is 1.818(2)–1.926(3) Å which is significantly shorter than 2.299(6)–2.348(6)Å found in the binuclear Ni complex [**Hiba! A könyvjelző nem létezik.**].

Table 1 Selected bond distances and angles

	Distance/Å					
Bond	**1**	**2**	**3**		**1**	**3**
M–N(4)	1.996(4)	1.938(2)	2.088(3)	M–Cl1	2.234(1)	2.539(1)
M–N(5)	1.854(4)	1.818(2)	1.926(3)	M–Cl2	2.264(2)	
M–N(6)	1.853(4)	1.839(3)	1.949(3)			
M–N(8)	1.918(3)	1.880(2)	1.955(3)			
N(4)–C(9)	1.309(6)	1.312(4)	1.295(5)			
C(10)–C(9)	1.472(7)	1.474(4)	1.484(6)			
N(5)–C(10)	1.322(6)	1.328(4)	1.319(5)			
N(5)–C(14)	1.341(6)	1.348(4)	1.341(5)			
C(14)–C(15)	1.464(7)	1.474(5)	1.467(6)			
N(6)–C(15)	1.321(6)	1.298(4)	1.304(6)			
N(7)–N(6)	1.335(5)	1.377(3)	1.352(4)			
N(7)–C(16)	1.348(5)	1.350(4)	1.345(5)			
N(8)–C(16)	1.371(6)	1.352(4)	1.352(5)			
N(8)–N(9)	1.341(5)	1.359(3)	1.360(5)			
N(9)–C(23)	1.310(6)	1.296(4)	1.307(6)			
N(4)–N(3)	1.398(5)	1.391(3)	1.390(4)			
N(3)–C(1)	1.301(6)	1.311(3)	1.302(5)			
C(2)–C(1)	1.476(7)	1.461(4)	1.463(5)			
C(1)–N(2)	1.345(7)	1.352(3)	1.351(5)			
N(1)–N(2)	1.378(6)	1.370(3)	1.367(5)			
N(1)–C(8)	1.303(7)	1.284(4)	1.301(6)			

	Angle/º		
Bond	**1**	**2**	**3**
N(6)–M–N(4)	164.06(16)	164.66(11)	156.34(13)
N(5)–M–N(8)	165.53(16)	165.42(11)	156.14(13)
N(5)–M–N(4)	80.55(17)	81.95(11)	78.55(13)
N(6)–M–N(5)	83.52(19)	83.12(12)	79.58(14)
N(6)–M–N(8)	82.07(16)	82.76(11)	79.24(14)
N(8)–M–N(4)	113.84(14)	111.87(11)	119.93(13)
N(6)–M–Cl(1)	91.19(13)	97.47(8)	97.39(10)
N(5)–M–Cl(1)	89.74(12)	79.63(8)	92.88(10)
N(8)–M–Cl(1)	89.25(11)	105.85(8)	100.64(9)

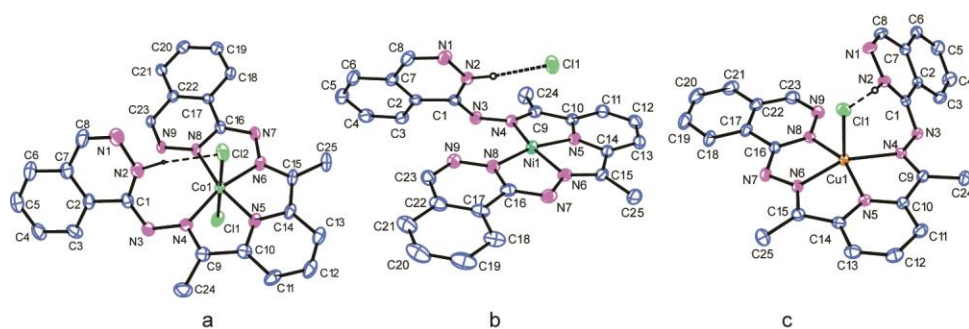|			
N(4)–M–Cl(1)	88.22(12)	83.33(7)	92.60(9)
N(6)–M–Cl(2)	88.78(13)		
N(5)–M–Cl(2)	90.65(13)		
N(8)–M–Cl(2)	90.35(11)		
N(4)–M–Cl(2)	91.91(12)		
Cl(1)–M–Cl(2)	179.60(6)		

Figure 1 Molecular diagrams and atom numbering schemes of **1** (a), **2** (b) and **3** (c). N–H...Cl hydrogen bonds are depicted by dotted lines.

Table 2 Hydrogen bond data for **1** and **2**

	D-H... A	H...A(Å)	D-H...A(°)	symmetry code
1	C21-H7.. Cl(2)^i	2.7315(9)	159	$i = x,1+y, z$
	C12-H12..Cl(1)^{ii}	2.80	150	$ii=x, -1+y, z$
2	C19-H9.. N(1)^i	2.4916(5)	165	$i = -x, -y, 1-z;$
	C25-H15.. N(3)^{ii}	2.4317(4)	174	$ii = 1-x, -y, 1-z$

Table 3 Geometry of stacking contacts for **2** and **3**

	(Ring 1), (Ring 2)	Ct–Ct distance (Å)	Dihedral angle (°)	symmetry code
2	(Ni1 N5 N6 C14 C15),	3.459(2)	1.9(1)	$i = 1-x, -y, 1-z$
	(Ni1 N6 N7 N8 C16)^i			$ii = -x, -y, 1-z$
	(N5 C10 C11 C12 C13 C14),	3.481(2)	2.1(2)	
	(N8 N9 C16 C17 C22 C23)^i			
	(N8 N9 C16 C17 C22 C23),	3.677(3)	0.4(2)	
	(C17 C18 C19 C20 C21 C22)^{ii}			
	(C17 C18 C19 C20 C21 C22),	3.659(3)	0	
	(C17 C18 C19 C20 C21 C22)^{ii}			
3	(Cu1 N5N6 C14C15),	3.499(2)	3.60(19)	$i = 2-x, -y, -z$
	(N8 N9C16C17C22 C23)^i			
	(Cu1 N6N7N8C16),	3.492(2)	0	
	(Cu1N6N7N8C16)^i			

| (N5C10C11C12C13C14), | 3.643(3) | 3.8(2) |
| (N8N9C16C17C22C23)[i] | | |

All three compounds possess extended π-system and thus have potential for stacking interactions. However this potential is manifested differently in compounds **1–3**, depending on the constraints imposed by the composition of the molecules. In **1**, the association of the molecules in the crystal is determined by the presence of the two chlorine atoms in the axial sites. Through the C–H...Cl hydrogen bonds (Table 2) molecules of the complex are arranged into molecular chain along the axis *b* (Fig 2). Solvent accessible area is situated between the two molecular chains. Due to the omission of the solvent molecules from the model, it was not possible to analyze fully the hydrogen-bonding interactions. However, the position of the solvent accessible void suggests that methanol has no role in the formation of molecular chains, but serves as a connection between the neighbouring chains.
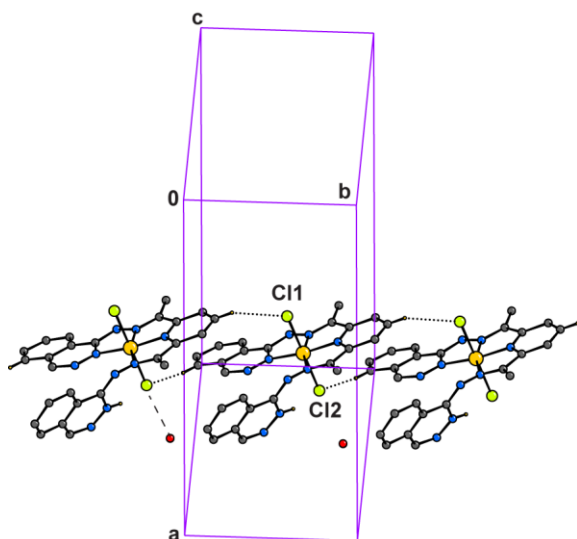

Figure 2 Part of the crystal structure of **1** showing association of molecules through the C-H...Cl hydrogen bonds, and formation of molecular chain along the axis b. Solvent accessible area is situated between the neighbouring chains. Centroid of the solvent accessible area is depicted as a red sphere.

Regarding the mode of the molecular association the most important difference between the **2** and **3** is the formation of metal–chlorine bonds. Namely, in **2**, the chlorine is at a significantly larger distances from the central metal [3.080(2) Å] than in **3**, [2.539(1) Å] and due to steric requirements the possibility of stacking arrangement between the two molecules is reduced. Therefore in **2** the packing of molecules in the crystal lattice is determined by the presence of the extended π system and the absence of significant steric restrictions to the mutual approach of neighbouring molecules. Hence, stacking interactions are formed, and two types of stacking interactions are observed. Interactions between the chelate rings lead to formation of molecular dimer with Ni...Ni distance of 3.964 Å. The dimers are further linked by the stacking interaction of the neighbouring phthalazine moieties to form a molecular chain along the *a* axis. Geometric parameters related to the stacking interactions and weak hydrogen bonds in the crystal structure of **2** are given in Table 3. In the crystal structure of **3**, molecules are linked into dimers through the chelate-chelate interactions [29], the distance between the neighbouring copper atoms being 4.49 Å. The dimers are arranged into chains along the *b* axis. Here too, solvent accessible area is located in the region between the molecular chains.

FT-IR spectral data

FT-IR spectral data of **1–3** are in the accordance with their molecular structure. The broad overlapping bands around 3408 cm^{-1} and 3033 cm^{-1} in the spectrum of the ligand, Hz$_2$DAP·2HCl are attributed to νNH vibrations [30], which

NH groups originate from protonation by HCl. Accordingly, they can form hydrogen bonds with the Cl⁻ counterions. In the spectra of the complexes **1**, **2** and **3** νN=C−NH appears in form of sharp bands at 3144, 3148 and 3150 cm^{-1}, respectively. The changes in the shape and position of the ligand bands in this region are related to the deprotonation of one of its NH-groups and the complexation.

Contrary to the compounds with Cu^{II}, Co^{III} and Ni^{II} where the ligand coordinates in its mono deprotonated form, with Zn^{II} a neutral complex is obtained with double deprotonated ligand molecule. In the agreement with the structure of the ligand, the arrangement of the ligand donor atoms around Zn^{II} centre is most probably square planar. It is reflected in the IR spectrum of **4** where one of the two bands around 1500 cm^{-1} has probably a considerable NH bending contribution. The intensity of the band at 1586 cm^{-1} is lower, and instead of two vibrations at 1500 and 1473 cm^{-1} in the spectrum of the free ligand, in the spectrum of **4** a very intensive band appears at 1488 cm^{-1}, in accordance with the presence of the ligand in the bisdeprotonated form. The characteristic bands in the range of 1600 – 1400 cm^{-1} for the ligand and **1–4** are presented in Table 4. The bands in the spectra of the complexes have been slightly shifted with the respect to the free ligand. The shoulder at 1562 cm^{-1} in the free ligand in spectra of **1–4** appears as a separate band and is shifted to lower energies as a result of coordination [31].

Table 4. Characteristic bands in the range of 1600 – 1400 cm^{-1}

Compound	C=C, C=N phthalazine, pyridine, cm^{-1}			
Hz$_2$DAP·2HCl	1584 vs	1562sh	1500m	1473 sh
1	1589 vs	1541 m	1504 s	1467 s
2	1587 vs	1548 w	1518 vs	1463 s
3	1589 vs	1547 w	1514 s	1467 s
4	1586 m	1541 m		1488 vs

Antimicrobial activity

Due to the fact that in molecular formulae of the investigated compounds chloride ion is included as co-ligand or counter ion, metal chlorides instead of acetates were used as controls. We also assumed that in such a low applied concentration methanol as crystal solvent does not influence the results.

All the tested compounds are insoluble in water, therefore were dissolved in DMSO for antimicrobial susceptibility testing. As pure DMSO showed some fungistatic and bacteriostatic activity (especially on *Bacillus* species) as is reported in the literature [32–33] the first probes and thus the high antimicrobial (bactericidal and fungicidal, fungistatic) activity of complexes in $1\cdot10^{-3}$ mol L^{-1} solutions in pure DMSO could be taken only as qualitative tests. Because of that, the stock solutions made with DMSO were diluted 10 times with deionized water and the same essays were repeated. After dilution, in solvent mixture of DMSO:H$_2$O = 1:9, the ligand (Hz$_2$DAP) and the solutions of Co^{II}, Ni^{II} and Cu^{II} chlorides were inactive towards used bacteria and fungi strains. Surprisingly, the ligand, Hz$_2$DAP, is practically inactive while its complexes **1–3** showed significant antimicrobial activity, especially on bacterial species. On the contrary, ZnCl$_2$ and its complex **4** enhanced the growth of *Candida albicans*, while the antibacterial activity of **4** is negligible. The minimal inhibition concentrations (MIC) of complexes, determined in DMSO solutions diluted with deionized water are presented in Table 5. For the most active Co^{III} complex (**1**) in cases of *Staphylococcus aureus* and *Micrococcus lysodeikticus* MIC extends to the value of $5\cdot10^{-6}$ mol L^{-1} (3 µg mL^{-1}) and is comparable with those obtained for standard antibiotics using some standard procedures for susceptibility testing by disk diffusion method [34] or dilution method in broth [35–36].

Table 5 Minimum inhibitory concentrations (MIC) in mol L^{-1} for **1–3**

Microorganism	1	2	3

Escherichia coli, ATCC 25922	$9 \cdot 10^{-6}$	$7 \cdot 1^{-5}$	$1 \cdot 10^{-5}$
Staphylococcus aureus, ATCC 25923	$5 \cdot 10^{-6}$	$5 \cdot 10^{-5}$	$1 \cdot 10^{-5}$
Bacillus subtilis, ATCC 6633	$1 \cdot 10^{-5}$	–	$5 \cdot 10^{-5}$
Bacillus cereus, ATCC 14579	$1 \cdot 10^{-5}$	–	$5 \cdot 10^{-5}$
Micrococcus lysodeikticus, ATCC 4698	$5 \cdot 10^{-6}$	$5 \cdot 10^{-5}$	$5 \cdot 10^{-5}$

On the basis of the experimental data the decreasing antibacterial activity against *Escherichia coli*, *Staphylococcus aureus* and *Micrococcus lysodeikticus* follows the order of the central metal ion $Co^{III} > Ni^{II} > Cu^{II} > Zn^{II}$. The decreasing activity could be related to the metal ions, as well as to the geometry around the metal center: octahedral> square pyramidal~ square planar, as well as to the presence of different number of Cl^- co-ligands.

Thermal analysis

The ligand is hygroscopic and loses water to about 150°C ($\Delta m = 6.2$ %). After water evaporation Hz$_2$DAP is stable to 180 ^{o}C. Its endothermic decomposition in nitrogen starts at 208 ^{o}C onset. Up to the first minimum the mass loss corresponds within experimental error to HCl evolution (exp. 13.3 %, calcd. 14.00 %). The decomposition at about 330 ^{o}C is almost complete, with a tar residue of 7 % at 400 ^{o}C.

Except **3** all the complexes crystallize with crystal solvent. **1** and **2** contain MeOH while **4** H$_2$O. However, according to TG measurements, **3** is highly hygroscopic. Thus, the first mass loss in all the compounds belongs to solvent evaporation. In **1** crystal MeOH in part evaporates from the samples during storage at room temperature (exp: ~1 %, calcd: 5.27 %).On the contrary, MeOH from **2** evaporates at surprisingly high temperature (191 ^{o}C onset, exp: 5.1 % ± 0.5 %, calcd: 5.59 %).The amount of hygroscopic water (exp: 6.3 %) in **3** agrees with two H$_2$O (calcd: 6.61 %) and departs below 100 ^{o}C. Water (exp: 3.9 %, calcd: 3.41%) from **4** evaporates completely also below 100 ^{o}C (Fig 3).
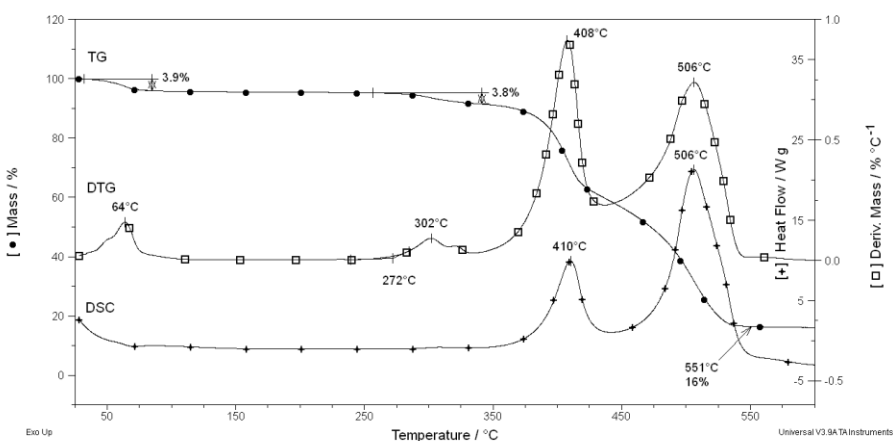

Fig 3 TG, DTG and DSC curves of **4** in nitrogen at a heating rate of 10 ^{o}C min^{-1}

The comparison of the decomposition mechanisms, given by the corresponding DTG curves, is presented in Fig. 4. After the solvent evaporation, in DTG curves of **2 – 4** in the temperature interval of 170 $^{\circ}$C – 350 $^{\circ}$C two more or less separated decomposition steps can be observed. The mass loss for the first step is ∼ 4 %. It is accompanied by an endothermic effect in **2** while in the other complexes the heat effect for the first step is hardly detectable. The mass loss in the following step is higher than 10 % and is accompanied by exothermic reactions. Above ∼400 $^{\circ}$C, the decomposition rate significantly decreases and in nitrogen is not complete to 700 $^{\circ}$C. The decomposition of **4**, except of H$_2$O evaporation, is exothermic in the whole temperature range and its degradation to ZnO (exp: 14.6 %, calcd: 15.39 % in air) or to Zn (exp: 9.4 %, calcd: 12.37 % in nitrogen) is complete around 550 $^{\circ}$C. The amount of the end products in air and nitrogen is somewhat less than the theoretical value probably because of the very high decomposition rate, but within experimental error agree with the theoretical values supporting thus the proposed composition of the complex.

To obtain more reliable structural information, controlled rate thermal analysis (CRTA) and coupled TG/MS measurements were carried out for compounds **2** and **4**.
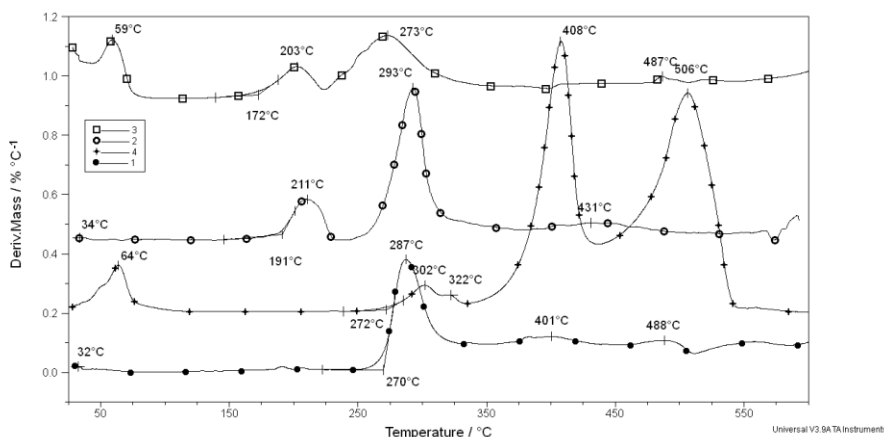

Fig. 4 DTG curves of compounds **1**, **2**, **3** and **4** in nitrogen at heating rate 10 $^{\circ}$C min^{-1}

The TG curves obtained by CRTA for **2** and **4** are presented in Fig. 5. According to the composition of **2**, the first mass loss is related to MeOH evaporation (exp. 5.1 %, calcd: 5.59 %). The next mass loss of 17.7 % corresponds to a fragment with a molecular mass of ∼100 and the next one to M_r∼ 28. According to the structure of the ligand these two fragments agree with departure of one phthalazine molecule that under isothermal conditions disintegrates into C$_8$H$_6$ and N$_2$.

After evaporation of crystal water, [Zn(Hz$_2$DAP-2*H*)] is stable to above 250 $^{\circ}$C. The molecular mass of the departing fragments with mass loss of ∼5 %, calculated on the basis of the proposed structure corresponds to N$_2$ evolution, while that of 37.7 % to fragment with M_r ∼ 200. On the basis of the structure of the ligand the mass loss most probably belongs to loss of two phthalazine molecules which, similarly to the compound **2**, disintegrate into N or N$_2$) and C$_8$H$_6$.The simultaneously lost phthalazine molecules refer to a more symmetrical structure of **4** compared to **2**.
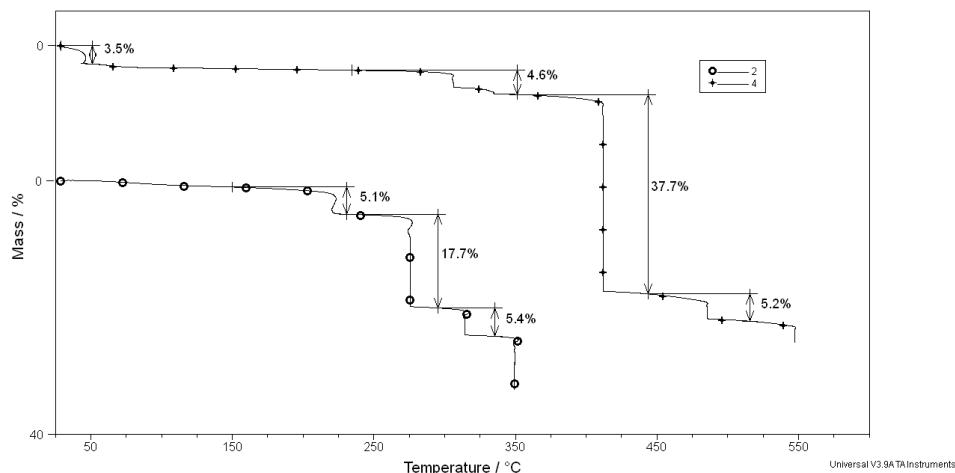
Figure 5 CRTA curves for complexes **2** and **4** in nitrogen

The decomposition mechanism of **4** is evaluated on the basis of evolved gas analysis (EGA), performed by coupled TG/MS measurements. Peaks for selected m/z data with the corresponding DTG curve are presented in Figs. 6 a and b. The first detected signals with the peaks maxima at 57 $^{\circ}$C and with $m/z = 18$ and 19 correspond to water evaporation, proposed also on the basis of the TG data. As the measurement was carried out in flowing N_2, the increase in N_2 signal level around 300 $^{\circ}$C and proposed on the basis of CRTA as N_2 evolution could not be unambiguously detected. At lower temperatures mainly fragments with lower molecular masses were detected which correspond to evolution of NH_3 ($m/z = 16$, 17) or methyl group ($m/z = 15$, 16). The intensity of the signal for CH_3^+ with $m/z = 15$ is several times less than that with $m/z = 16$, while the signal intensity of the fragment with $m/z = 17$ (NH_3^+) is somewhat higher than that with $m/z = 16$ (CH_4^+ and NH_2^+). A group of signals at 445 $^{\circ}$ is found in the range of $m/z = 38 - 42$ with the most intensive signal for $m/z = 41$. The signal intensity ratio corresponds for C_3H_3N (acetonitrile) evaporation [37]. The acetonitrile is most probably formed by the scission of the bond between the nitrogen atoms of the hydrazine group and that with the pyridine ring. The peak with the far highest intensity is detected for $m/z = 118$ with peak temperature at 450 $^{\circ}$C. It can be related to phthalazine group only, despite that it is not detected in the phthalazine mass spectrum, while in the spectrum of the hydralazine appears with a very low intensity. However, it is the strongest peak in the 1H-indazole spectrum [37] and can be formed easily from the phthalazine ring during the thermal decomposition of phthalazine complexes. Some fragments like $m/z = 77$ appear with maxima at two temperatures. This fragment, though with very low signal intensity, is present in both pyridine and phthalazine spectrum [37]. As the peak at 445 $^{\circ}$C belongs to phthalazine ring fragmentation, the peak at the higher temperature (peak maximum~490 $^{\circ}$C) can be related to pyridine fragmentation (Fig. 6b).

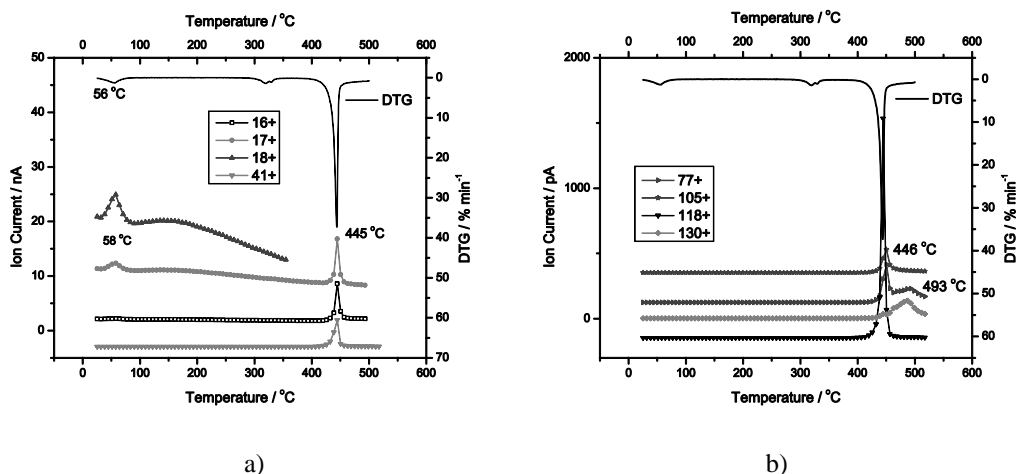a)   b)

Fig 6 Selected TG/MS curves for complex **4**

As the evaporation temperature of MeOH in **2** seems too high, TG/MS measurements were used to verify its presence. Peaks for $m/z = 31$ and $m/z = 32$ with maxima at ~ 200 $^{\circ}$C detected in an intensity ratio of about 100/60 respectively unambiguously validate the evaporation of MeOH [37]. The departing fragments during the decomposition of **2** are similar to those observed during the decomposition of **4** and almost all appear in the mass spectrum of the phthalazine and pyridine, *i.e.* the ligand components. However, the intensity ratio of these peaks is significantly different from that in the phthalazine or pyridine spectrum. The different intensity ratio can be attributed to the coordination of the ligand to the metal centre and to their thermal fragmentation. On the contrary, the signal intensity ratio of the evolved solvents and those of the volatile compounds with lower molecular masses, formed during the decomposition is very similar to those found in data bases.

Conclusions

The bis(phthalazine-1-hydrazone)-2,6-diacetylpyridine ligand coordinates in (NNNN) coordination mode in all four complexes. In compounds with Co^{III}, Ni^{II} and Cu^{II} the ligand is coordinated in its mono-deprotonated form. Nonetheless, the geometry of the complexes is different. With Co^{III} an octahedral complex is formed, with two chlorides in axial positions, while the geometry around Ni^{II} and Cu^{II} metal centres is square pyramidal with chloride ion at the top of the pyramid. The structure of the Zn^{II} complex is determined on the basis of the IR spectral and thermoanalytical data. The (NNNN) coordination mode of the ligand is characteristic for Zn complex, too, but it is coordinated in bisdeprotonated form, giving thus the neutral complex of [Zn(Hz$_2$DAP-2H)]·H$_2$O. The antimicrobial activity of the complexes [Co(Hz$_2$DAP-H)Cl$_2$]·MeOH, [Ni(Hz$_2$DAP-H)]Cl·MeOH and [Cu(Hz$_2$DAP-H)Cl] against *Escherichia coli*, *Staphylococcus aureus* and *Micrococcus lysodeikticus* is significant, but surprisingly the activity of the ligand is negligible against all strains. On the contrary, [Zn(Hz$_2$DAP-2H)]·H$_2$O promotes the growth of *Candida albicans*. The activity of the complexes is different and could be related to the metal ions, as well as to the different geometry around the metal centres. The thermal decomposition pattern due to different structures of the compounds is also different. TG/MS measurements supported the presence of the crystal solvents. The signal intensity ratio of the evolved solvents and those of the volatile compounds with lower molecular masses, formed during the decomposition is very similar to those found in data bases. Significant fragments in the mass spectra of the phthalazine and pyridine were detected in all tested compounds. However, as a result of different structures and thermal fragmentation, the intensity ratios are very different.

Literature

1. Druey J, Marxer A. Hypotensive Hydrazinophthalazines and Related Compounds. J Med Pharm Chem. 1959; 1:1-21.

2. Thompson LK, Mandal, SK, Charlan JP, Gabe EJ. Magnetism and structure in a series of halogen and hydroxo-bridged binuclear copper(II) diazine complexes. Can J Chem. 1988; 66:348-54 and references therein.

3. Mandal SK, Thompson LK, Newlands MJ, Charland JP, Gabe EJ. Binuclear copper(II) complexes of some sexadentate phthalazinehydrazone ligands with strong antiferromagnetic exchange. Inorg Chim Acta. 1990;178: 169-78.

4. El-Sherif AA, Shoukry MM, Abd-Elgawad MMA. Spectrochim Acta A. Synthesis, characterization, biological activity and equilibrium studies of metal(II) ion complexes with tridentate hydrazone ligand derived from hydralazine. 2012; 98:307-21.

5. Popov LD, Levchenkov SI, Shcherbakov IN, Kogan VA, Tupolova YuP. 1'-Phthalazine hydrazone of diacetyl monooxime and its complexes with transition metals. Russ J Gen Chem. 2010; 80:471-78.

6. Popov LD, Mishchenko AV, Tupolova YuP, Levchenkov SI, Minin VV, Ugolkova EA, Efimov NN, Lukov VV, Shcherbakov IN, Kogan VA, Zubenko AA, Askalepova OI. Synthesis, Structure, and Complexing Ability of Hetarylhydrazones of Glyoxylic Acid. Russ J Gen Chem. 2011; 81:1346-53.

7. Popov LD, Shcherbakov IN, Levchenkov SI, Tupolova YuP, Burlov AS, Aleksandrov GG, Lukov VV, Kogan VA. Transition Metal Complexes with 2-(*N*-Tosylamino)benzaldehyde 1-Phthalazinylhydrazone. Russ J Coord Chem. 2011; 37:483-91.

8. Hoover JM, Dipasquale A, Mayer JM, Michael FE. Platinum-Catalyzed Intramolecular Hydrohydrazination: Evidence for Alkene Insertion into a Pt-N Bond. J Am Chem Soc. 2010; 132:5043-53.

9. Shoukry AA, Shoukry MM. Coordination properties of hydralazine Schiff base: Synthesis and equilibrium studies of some metal ion complexes. Spectrochim Acta A. 2008; 70:686-91.

10. Kogan VA, Levchenkov SI, Popov LD, Shcherbakov IA. 1-Hydrazinophthalazine based hydrazones and their transition metal complexes: Structure and Biological Activity. Russ J Gen Chem. 2009; 79:2767-2775.

11. Paolucci G, Stelluto S, Sitran S, Ajò D, Benetollo F, Polo A, Bombieri G. Polynuclear transition metal complexes. Inorg Chem Acta. 1992; 193: 57-75.

12. Lima NGPB, Lima IPB, Barros DMC, Oliveira TS, Raffin FN, de Lima e Moura TFA, Medeiros ACD, Gomes APB, Aragão CFS. Compatibility studies of trioxsalen with excipients by DSC, DTA, and FTIR. J Therm Anal Calorim. 2013; DOI 10.1007/s10973-013-3216-y.

13. Tita B, Jurca T, Tita D. Thermal stability of pentoxifylline: active substance and tablets. J Therm Anal Calorim. 2013; 113:291–99.

14. Veronez IP, Daniel JSP, Garcia JS, Trevisan MG. Characterization and compatibility study of desloratadine. J Therm Anal Calorim. 2013; DOI 10.1007/s10973-013-3271-4.

15. Wesolowski M, Rojek B. Thermogravimetric detection of incompatibilities between atenolol and excipients using multivariate techniques. J Therm Anal Calorim. 2013;113:169–77.

16. Alghool S, Abd El-Halim HF, Abd El-sadek MS, Yahia IS, Wahab LA. Synthesis, thermal characterization, and antimicrobial activity of lanthanum, cerium, and thorium complexes of amino acid Schiff base ligand. J Therm Anal Calorim. 2013; 112:671–81.

17. Finn RK. Theory of agar diffusion methods for bioassay. Anal Chem. 1957;31:975–977.

18. Osowole AA, Kempe R, Schobert R. Synthesis, spectral, thermal, *in-vitro* antibacterial and anticancer activities of some metal(II) complexes of 3-(-1-(4-metoxy-6-methyl-2-pyrimidinylimino)methyl-2-napthol. International Research Journal of Pure and Applied Chemistry. 2012; 2: 105-129.

19. CrysAlis RED Versions 1.171.32.5: Oxford Diffraction Ltd., Oxford Diffraction, 2007.

20. Altomare A, Cascarano G, Giacovazzo C, Guagliardi A. Completion and refinement of crystal structures with SIR92. J Appl Crystallogr. 1993; 26: 343-350.

21. Farrugia LJ. WinGX suite for small-molecule single-crystal crystallography. J Appl Crystallogr. 1999; 32: 837-838.
22. Sheldrick GM. SHELX97, Programs for crystal structure analysis. University of Göttingen: Göttingen, Germany, 1997.
23. Spek AL. PLATON, A Multipurpose Crystallographic Tool, Utrecht University, Utrecht, The Netherlands, 1998.
24. Nardelli M. PARST95 - an update to PARST: a system of Fortran routines for calculating molecular structure parameters from the results of crystal structure analyses. J Appl Crystallogr. 1995; 28: 659.
25. Watkin DM, Pearce L, Prout CK. Molecular Graphics Package, Chemical Crystallography Laboratory, University of Oxford, 1993.
26. Farrugia LJ. ORTEP-3 for Windows: a version of ORTEP-III with a Graphical User Interface (GUI). J Appl Cryst. 1997; 30: 565.
27. Suzuki T, Morikawa A, Kashiwabara K. Preparation and Characterization of Nickel(II), Palladium(II), and Platinum(II) Complexes Containing (2-Aminoethyl)dimethylphosphine or the Related Didentate Phosphine Ligands. Bull Chem Soc Jpn. 1996; 69: 2539-2548.
28. Allen FH. The Cambridge Structural Database: a quarter of a million crystal structures and rising. Acta Cryst. 2002; B58: 380-388.
29. Sredojević DN, Tomić ZD, Zarić SD. Evidence of Chelate-Chelate Stacking Interactions in Crystal Structures of Transition-Metal Complexes. Crystal Growth & Design. 2010; 10: 3901-3908.
30. Katritzkmy AR, Phil D. The infrared spectra of heteroaromatic compounds. Quart Rev Chem Soc. 1959; 13:353–373.
31. Paolucci G, MarangoniG, BandoliG, Clemente DA. Reactivity of uranyl ion with quinquedentate chelating hydrazine derivatives. Part 1. 2,6-Diacetylpyridine bis(2'-pyridylhydrazone). JCS Dalton 1980; 459–466.
32. http://www.dmso.org/articles/information/herschler.htm
33. Hayen KC. Influence of DMSO on antifungal activity during susceptibility testing *in vitro*. Diagn Microbiol Infect Dis. 2013; 75: 60-63.
34. Bell SM, Pham JN, Nguyen TT. Antibiotic Susceptibility Testing by the CDS Method, Sixth Edition 2013, The Antibiotic Reference Laboratory, South Eastern Area Services, Randwick, Australia http://web.med.unsw.edu.au/cdstest
35. Reimer LG, Stratton CW, Reller LB. Minimum inhibitory and bactericidal concentrations of 44 antimicrobial agents against three standard control strains in broth with and without human serum. Antimicrob Agents Chemother, 1981; 19:1050-1055.
36. Andrews JM. Determination of minimum inhibitory concentrations. J Antimicrob Chemother. 2001; 48 Suppl. S1:5-16.
37. http://webbook.nist.gov/ 21.08.2013.